ACS APPLIED MATERIALS & INTERFACES

Research Article

www.acsami.org

Diamond Network: Template-Free Fabrication and Properties

Hao Zhuang,[†] Nianjun Yang,[†] Haiyuan Fu,[†] Lei Zhang,[†,‡] Chun Wang,[§] Nan Huang,[§] and Xin Jiang*[,†,§]

[†]Institute of Materials Engineering, University of Siegen, Paul-Bonatz-Str. 9-11, 57076 Siegen, Germany

[‡]Peter Grünberg Institute and Ernst Ruska-Centre (ER-C) for Microscopy and Spectroscopy with Electrons, Forschungszentrum Jülich GmbH, Jülich 52425, Germany

[§]Shenyang National Laboratory for Materials Science, Institute of Metal Research (IMR), Chinese Academy of Sciences (CAS), No. 72 Wenhua Road, Shenyang 110016 China

Supporting Information

ABSTRACT: A porous diamond network with three-dimensionally interconnected pores is of technical importance but difficult to be produced. In this contribution, we demonstrate a simple, controllable, and "template-free" approach to fabricate diamond networks. It combines the deposition of diamond/β-SiC nanocomposite film with a wet-chemical selective etching of the β-SiC phase. The porosity of these networks was tuned from 15 to 68%, determined by the ratio of the β-SiC phase in the composite films. The electrochemical working potential and the reactivity of redox probes on the diamond networks are similar to those of a flat nanocrystalline diamond film, while their surface areas are hundreds of times larger than that of a flat diamond film (e.g., 490-fold enhancement for a 3 μm thick diamond network). The marriage of the unprecedented physical/chemical features of diamond with inherent advantages of the porous structure makes the diamond network a potential candidate for various applications such as water treatment, energy conversion (batteries or fuel cells), and storage (capacitors), as well as electrochemical and biochemical sensing.

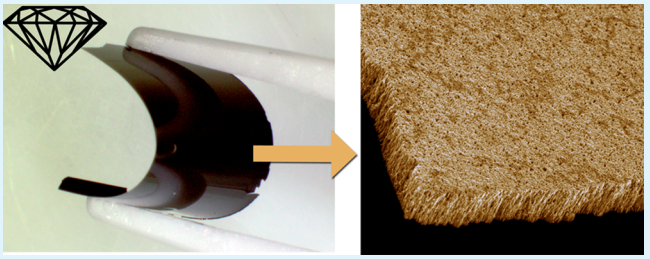

KEYWORDS: *diamond, porous, electrochemistry, composite, SiC*

INTRODUCTION

Porous materials are of great interest for material scientists, chemists and biochemists due to their huge "extra spaces" and large surface areas in comparison to their bulk flat counterparts. Depending on different sizes and natural properties of the pores, the transfer/movement of atoms, ions, molecules, and particles throughout the pores are possible, enabling us to monitor, determine, and investigate their interactions. On the basis of this concept, applications such as water treatment, energy conversion (e.g., batteries or fuel cells), energy storage (e.g., capacitors), sensors, and so on have benefited greatly.[1−5]

Various porous structures from different materials (e.g., polymer, silica, metals, Al_2O_3, etc.) have thus been produced with different strategies.[4−10] The fabrication of porous structures from diamond, an important technical material with superlative physical qualities,[11,12] however, still remains challenging. Until today, only a few approaches are available, for instance, diamond coating of porous template[13−16]/carbon nanotubes[17]/opal matrices,[18,19] dry etching of diamond through Al_2O_3 template,[20] colloidal crystal templating,[21] and so on. Nonetheless, the current approaches are far away from industrial applications because of the involvement of complex templates or expensive dry etching processes. Moreover, to our best knowledge no work has dealt with a template-free approach for fabricating a porous diamond with three-dimensionally interconnected (both vertically and horizontally) pores, the so-called "diamond network".[22] Such a network is highly desired because it allows the porous diamond to possess a high permeability in liquid media. Its successful fabrication will thus open doors to a plethora of applications through utilizing the unprecedented physical/chemical properties of diamond and the inherent advantages of the porous structure.

Herein, we demonstrate a new and controllable method to fabricate diamond networks without involving any templates. Tunable pore volume of the networks, namely porosity, ranging from 15 to 68% was achieved and resulted in a significant enhancement of their surface areas. For instance, a surface area enhancement of ∼490-fold was achievable for a diamond network with a 3.0 μm thickness in comparison with a flat nanocrystalline diamond film. Further electrochemical characterization indicates that the diamond networks possess similar electrochemical properties (i.e., electrochemical working potential and redox activities) to those of bulk diamond.

EXPERIMENTAL SECTION

Deposition of Nanocrystalline Diamond/β-SiC Composite Films. The composite films were deposited on (100) Si wafers and (0001) 2H-SiC wafers by microwave plasma chemical vapor

Received: December 15, 2014
Accepted: February 20, 2015
Published: February 20, 2015

DOI: 10.1021/am508851r
ACS Appl. Mater. Interfaces 2015, 7, 5384−5390

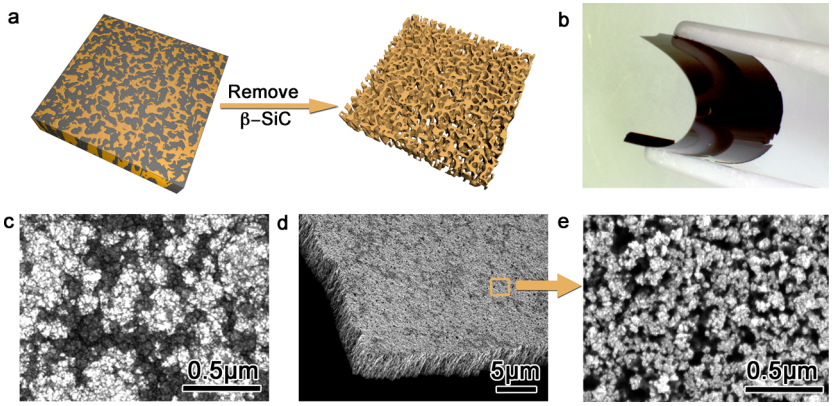

Figure 1. (a) Illustration of fabricating a diamond network from the composite film: the gray phase (β-SiC) is removed, leaving a yellow porous phase (diamond). (b) An optical photo of a flexible freestanding diamond network film. (c) SEM surface images of a nanocrystalline diamond/β-SiC composite film deposited with TMS/CH_4 ratio of 1.5%. (d) Diamond network fabricated by etching the β-SiC phase from composite film shown in image c. (e) High-magnification SEM images of the surface of the film shown in image d.

deposition (CVD) technique (ASTeX A5000). To enable the growth of nanocrystalline diamond/β-SiC composite films, a low microwave power of 700 W was applied to ignite and sustain the plasma. The deposition was carried out at constant gas pressure of 15 Torr and a substrate temperature of 800 °C. H_2, CH_4, and tetramethylsilane (TMS) are the main precursors used for the growth of composite films. The total gas flow rate was kept at 400 sccm (standard cubic centimeter per minute) and the concentration of CH_4 was maintained at 2%. The TMS to CH_4 ratios were varied from 0.8 to 2.2% to obtain different diamond/β-SiC ratios in the composite films with the other parameters being constant. The samples used for the electrochemical characterization were doped with boron by the addition of trimethylborane (TMB, B/C = 3000 ppm) during the growth process.

Etching of the Composite Films. Etching of the composite film was carried out in the mixture of HF (40%, Sigma-Aldrich) and HNO_3 (65%, Th. Geyer GmbH) with a volume ratio of 3:1. The whole process was carried out in a bath at 80 °C for different times (e.g., 12–72 h). After etching, the samples were rinsed in distilled water to remove the residual acidic species. Then the samples were dried in an oven at 105 °C for at least 4 h.

Characterization of Diamond Networks. The surface and cross-sectional morphologies of the composite films and the diamond networks were imaged by scanning electron microscope (SEM, Zeiss Ultra 55) and transmission electron microscope (TEM, Philips CM20). To access the information on the surface fraction of β-SiC, the SEM images of the composite films were analyzed in the image analysis software. The area of every β-SiC domain in the image was measured and summed up. Then the sum of the β-SiC area was divided by the area of the total image to obtain the surface ratio of β-SiC in the composite film. For preparing the sample for the TEM analysis, the freestanding diamond network was attached a copper grid and thinned using ion milling. The electrochemical characterization of the diamond network was carried out using a CHI 660E electrochemical workstation (Shanghai, CH Instruments, Inc., Austin, TX) with a three-electrode configuration. Either a flat diamond or a diamond network was used as the working electrode. The platinum wire acted as the counter electrode, and the Ag/AgCl electrode acted as the reference electrode.

RESULTS AND DISCUSSION

Our method, which is schematically shown in Figure 1a, is simple and straightforward. Through wet-chemically boiling of diamond/β-SiC composite films, the β-SiC phase is selectively removed from the composite film, leaving the diamond phase porous. The mixture of HF and HNO_3 was chosen as the etching. It has been reported to etch β-SiC whiskers without the aids of any external sources (i.e., electric fields, UV illuminations, etc.).[23] During the etching process, the following reactions take place continuously:[23,24]

$$SiC + 2HNO_3 + 2H_2O \rightarrow 2HNO_2 + 4OH^- + SiC^{4+} \quad (1)$$

$$SiC^{4+} + 4OH^- \rightarrow SiO_2 + CO_2 + 2H_2 \quad (2)$$

$$SiO_2 + 6HF \rightarrow H_2SiF_6 + 2H_2O \quad (3)$$

The porosity of diamond networks is thus possible to be controlled if the distribution and ratio of β-SiC phase in the composite film are variable. Using CVD, we were actually able to precisely control the ratio, distribution, and crystallinity of both diamond and β-SiC phases.[25−27]

In a separate experiment, the etching behavior of β-SiC with different crystallinity has been explored. It was revealed that the etching rate of β-SiC is crystallinity-dependent, which is in accordance to the literature.[24] We are able to fully etch away the nanocrystalline β-SiC film with a thickness of ~600 nm in 3 h, giving an etching rate of ~200 nm/h. The etching of microcrystalline β-SiC film is much slower and eventually stops after 24 h. To achieve an efficient and full removal of the β-SiC phase, a diamond/β-SiC composite film system with nanocrystalline β-SiC phase was thus chosen as the starting material for the fabrication of diamond networks.

It is noteworthy that the conventional supporting Si substrate (used for the growth of composite films) was quickly removed in the first minute of the etching process. This is because the etching resistivity of Si is lower than that of β-SiC. A freestanding diamond network can therefore be obtained in this way. Due to its low thickness (4 μm) and the existence of pores, the diamond network shows certain flexibility; one such diamond network with a size of 1 × 0.5 cm^2 is depicted in Figure 1b. Because the films are thin (4 μm), they might break into pieces when a force is applied to them during processing (i.e., removing from the etching solution, washing in water, drying, etc.). Such freestanding films are nevertheless transportable. Furthermore, it is also possible to directly obtain such a diamond network with substrate support for better handling. In this case, the substrate (used for the deposition of the composite films) should not be etched away during the etching process. In this regard, materials (e.g., diamond, single crystalline SiC, etc.) with higher etching resistivity than nanocrystalline SiC have been used for the deposition of

DOI: 10.1021/am508851r
ACS Appl. Mater. Interfaces 2015, 7, 5384−5390

composite films, and diamond networks directly with substrate support after etching have been obtained.

Figure 1c and Figure S1a (in Supporting Information) show the SEM images of one diamond/β-SiC nanocomposite film, revealing its surface morphology. This composite film is applied for the fabrication of diamond network in Figure 1b. Due to different secondary electron yields of diamond and β-SiC, the film contains bright and dark regions, which correspond to nanometer sized diamond and β-SiC crystals, respectively.[26] This film underwent a 72 h etching process to obtain the diamond network. Figure 1d,e depicts SEM images of the final structure of the diamond network in a side view and a top view (see also Figure S1b in Supporting Information for a low magnification image). The thickness of this diamond network is about 4 μm. The pores are homogeneously distributed in the film but without uniform size and shape. This is due to the random growth of β-SiC phases. Nevertheless, the size of all the pores is tens of nanometers, suggesting that diamond network belongs to the macroporous material.[28]

To gain more insight into the etching process of the composite film, its cross-section at different etching durations was monitored by SEM, as shown in Figure 2. The left column

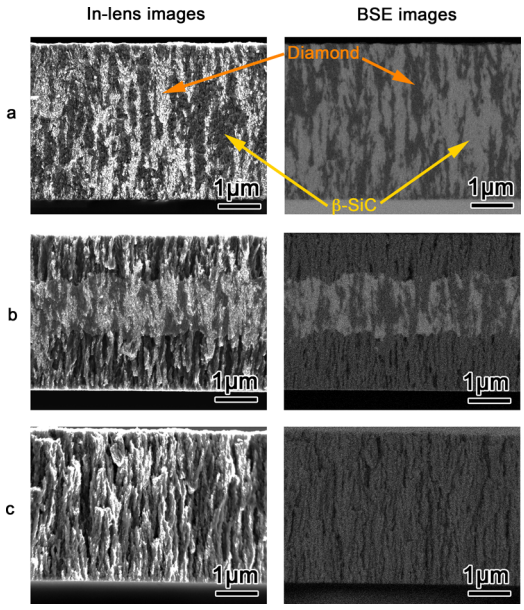

Figure 2. Cross-sectional SEM images of the composite film (TMS/CH_4 = 1.5%) with different etching time, both in-lens secondary electron images (images in the left column) and BSE images (images in the right column) were taken: (a) original composite film without etching, (b) after 48 h etching, and (c) after 72 h etching.

of Figure 2 depicts the in-lens secondary electron images, and the right column shows the backscattered electron (BSE) images. During etching, the β-SiC phase was gradually removed from both sides (Figure 2b). After 72 h, the β-SiC phase was completely removed from the film, giving an etching rate of ~50 nm/h. Because the β-SiC phase in the center of the film was only etched away by the diffusion of etching reagents through the pores formed in the etching process, its removal indicates that the pores in the diamond network are continuous. These pores are thus permeable in water. Moreover, owing to the random growth nature of β-SiC, the β-SiC phase is clearly observed to interconnect with each other in the composite film (Figure 2a). As a result, interconnected pores (both vertically aligned and horizontally connected) can be produced after etching, indicating the successful fabrication of diamond network.

Raman spectra of a diamond/β-SiC nanocomposite film before (Figure 1c) and after the etching process (Figure 1e) were recorded, as shown in Figure 3. Due to its poor

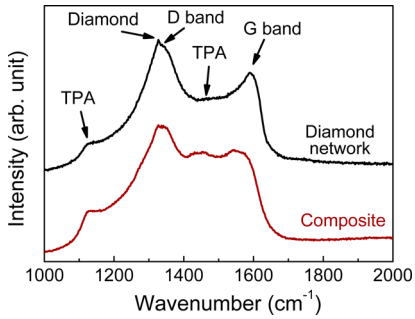

Figure 3. Raman spectra of the composite film and the diamond network.

crystallinity, the Raman signal of the β-SiC phase could not be distinguished in the carbon-rich atmosphere.[26] For both of the samples, peaks at 1332 cm^{-1} (corresponding to diamond), at ~1150 and ~1460 cm^{-1} (corresponding to trans-polyacetylene, TPA), and at ~1350 and ~1520 cm^{-1} (corresponding to D band and G band of amorphous carbon, respectively) are present. The strong D and G bands and the existence of the TPA Raman peak strongly indicate that the diamond phase is composed by nanocrystalline diamond.[29] This is also in good accordance with the SEM (Figure 1c,e) and TEM (shown below) observations, in which, nanometer sized diamond crystals present. Moreover, the similarities of the Raman spectra before and after etching implies the structure of the diamond phase in the film did not change during etching. A slight change in the relative intensities of the above peaks is probably due to the alteration of the diamond fraction in the film before and after etching. This is because both of the amorphous phase and TPA exist in the grain boundaries of the SiC region. They were removed during the etching process, leading to the reduction of their Raman signal in the diamond network.

To obtain more detailed structural information on the diamond network, its TEM images are shown in Figure 4. As shown in Figure 4a, the as-grown diamond/β-SiC composite film is dense and pinhole free. The crystal size of both diamond and β-SiC is less than 50 nm. The characteristic diffraction rings (Figure 4a, inset) indexed to diamond and β-SiC indicate the composition of polycrystalline diamond and β-SiC phases in the film. Typical high-resolution TEM (HRTEM) images of β-SiC and diamond crystals are shown in Figure S1c,d (Supporting Information) and show characteristic lattice fringes of β-SiC and diamond with the interplanar spacing of their {111} planes of 0.252 and 0.206 nm, respectively. Figure 4b shows the TEM image of the diamond network. The inset shows the corresponding selective area electron diffraction (SAED) pattern. The disappearance of the diffraction rings of β-SiC in the SAED pattern confirms the full removal of β-SiC. In accordance with Figure 1e, the pores are homogeneously distributed in the film. TEM images of the diamond network with higher magnifications are shown in Figure 4c,d. It is clearly observed that the shape of the pores is irregular. The majority of the pores are ~50 to ~200 nm in diameter. A few pores with

DOI: 10.1021/am508851r
ACS Appl. Mater. Interfaces 2015, 7, 5384−5390

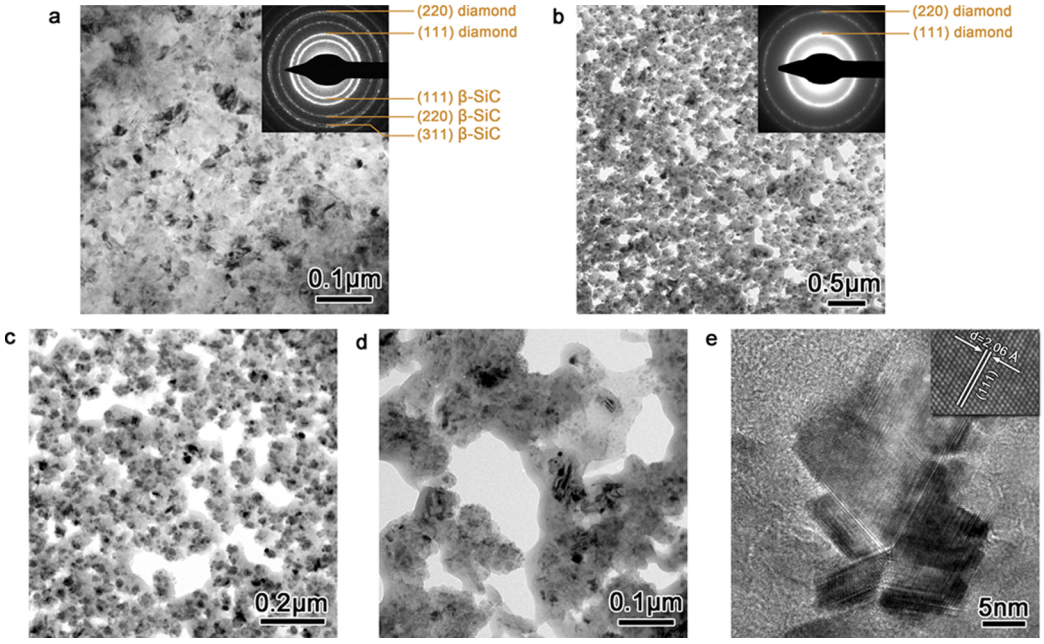

Figure 4. (a) TEM images of the composite film deposited with TMS/CH_4 ratio of 1.5%; (b) low-magnification TEM images of the diamond network fabricated from image a; (c and d) high-magnification TEM images of image b; (e) HRTEM image of one diamond crystal in the diamond network.

a size smaller than 50 nm exist as well. This is due to the nanometer- to micrometer-scale distribution of the β-SiC phase in the composite film, evidenced from Figure 1c and from Figure S1a (Supporting Information, dark regions).

Figure 4e depicts HRTEM image of one diamond crystal in the diamond network, showing clear lattice fringes. The interplanar spacing is measured as 0.206 nm, which is indexed to the {111} diamond planes. Typical planar defects (twins or stacking faults) parallel to the {111} crystal planes are also observable in the crystal. No differences or damage was found between this diamond crystal and the one in the composite film (Figure S1d, Supporting Information). This fact proves that the diamond crystals have not been damaged during the etching process, which is in good accordance with the Raman results shown in Figure 3.

While fabricating porous materials, especially networks, the tunability of porosity always requires special care. Until now, no reports were able to deal with porous diamond with tunable porosities. By using our approach, however, we successfully controlled the porosity of diamond networks. It was achieved by adjusting the ratio of β-SiC phase in the diamond/β-SiC composite films. According to our previous results, the ratio of β-SiC phase has been precisely controlled by varying the fed gas composition (TMS/CH_4 ratios) during the growth of composite films.[26,30−32] Figure S2 in Supporting Information shows three composite films deposited with different diamond/β-SiC ratios. SEM images of the diamond networks generated from these films are shown in Figure 5a−c. For all diamond networks produced, the shapes of pores are irregular. Apparently, the pore size and porosity vary greatly in different samples. The pore size increases from tens of nanometers to hundreds of nanometers with an increase of TMS/CH_4 ratios from 0.8 to 2.2%. Because all pores come from the removal of β-SiC from the film, the porosity of diamond networks can be estimated by evaluating the volume fraction of β-SiC phase in the diamond/β-SiC composite film. The growth of diamond/β-SiC composite films is known to be a competition process.[32]

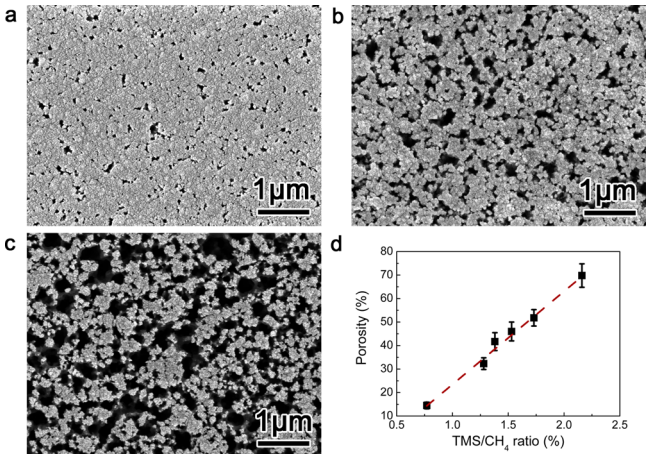

Figure 5. SEM surface images of diamond networks having different porosities fabricated from composite films deposited with the TMS/CH_4 ratios of (a) 0.8, (b) 1.3, and (c) 2.2%. (d) Plot of the porosity of the diamond networks as a function of the TMS/CH_4 ratios used for the deposition of composite films.

An equilibrium in the growth of diamond and β-SiC phases can be quickly established after the initial nucleation stage (within the first 100 nm).[32] As a result, when the TMS/CH_4 ratio and other deposition conditions are not changed, the diamond/β-SiC ratio in the composite film will remain constant throughout the deposition process.[32] Such a growth feature allows us to estimate the volume fraction of β-SiC by only measuring the fraction of β-SiC on the surface of the composite films (see Experimental Section for details). In this way, the porosities were estimated to be 15, 30, and 68% for diamond networks shown in Figure 5a−c, respectively. It is noteworthy that, when the porosity reaches 68% (Figure 5c), the mechanical stability of the film becomes poor. Besides those shown in Figure 5a−c, diamond networks with other porosities have been also fabricated. Figure 5d summaries their porosities as a function

DOI: 10.1021/am508851r
ACS Appl. Mater. Interfaces 2015, 7, 5384−5390

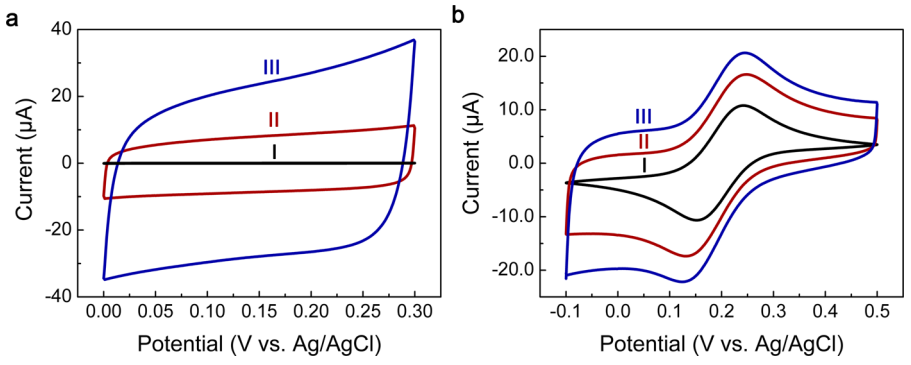

Figure 6. Electrochemical properties of a flat diamond film (I), DN16 (II), and DN64 (III). (a) Cyclic voltammetry in 0.1 M H_2SO_4 at a scan rate of 0.1 V/s. (b) Cyclic voltammetry in 1.0 mM $[Fe(CN)_6]^{3-/4-}$ in 0.1 M KCl at a scan rate of 0.1 V/s.

Table 1. Summary of Porous Diamond Fabricated Using Different Techniques

porous diamond	method	template-free	controllable porosity	film thickness (μm)	normalized surface area enhancement ($/\mu$m)	ref
diamond foam	coating on SiO_2 sphere	no	no	4	~25[a]	33
honey comb	reactive ion etching	no	yes	0.5	21[b]	20
diamond/CNT	coating on CNT	yes	no	5−40	10−30	17
diamond on porous material	coating on porous pt or si	no	yes			13, 16
nanoporous diamond	burning in air	yes	no			22
diamond network	wet etching	yes	yes	3	53−163	this work

[a]This value was obtained by dividing the double layer capacitance of the diamond foam by the typical double layer capacitance of flat diamond film (4 $\mu F/cm^2$). [b]This value was obtained from the direct geometrical calculation upon the regular pore shape. However, the double layer capacitance of the film increases by 200-fold, which might be due to the damage of the diamond surface during etching process.

of TMS/CH_4 ratio employed during the growth of the diamond/β-SiC composite films. The porosity increases linearly with increasing TMS/CH_4 ratios used for the deposition of the composite film. As a result, wide-range tunability (~15 to ~68%) in the porosity of the diamond network has been achieved in the present study.

All the diamond networks shown above are undoped. It is well-known that, one promising application of porous materials is as electrodes for electrochemical applications like super-capacitors, catalyst support, batteries, etc., owing to their large surface area. To adopt the diamond networks for such applications, however, a good conductivity represents a prerequisite. To obtain conductive diamond networks, we doped the composite films with boron by introducing trimethylborane (TMB) during growth. However, the presence of TMB in the gas phase was found to affect the growth of both diamond and β-SiC phases[34] because its amount is comparable to that of TMS in the gas phase. More detailed information in this aspect will be reported elsewhere. In the present work, we applied a B/C ratio of 3000 ppm in the gas phase to maintain the growth of nanocrystalline composite film with similar structure to that of the undoped composite films. As a result, the boron-doped diamond networks with similar structure to those of undoped diamond networks are obtained. Although this doping level is relatively low for achieving a high electrical conductivity of diamond, a sheet resistance lower than 300 Ω/sq was obtained for all the films. This value suggests their suitability as electrodes for electrochemical applications. Prior to the deposition of the diamond/β-SiC composite films, a boron-doped diamond layer with a thickness of ~800 nm was deposited. This pure diamond layer acts as a current collecting layer and prevents leakage of electrolyte on the substrate as well. The SEM image of one such film is shown in Figure S3 in Supporting Information.

Electrochemical techniques were applied to get a deep insight into electrochemical properties of diamond networks, such as their effective surface area, potential windows, and redox activities.[17,20,33] The effective surface areas of the diamond networks were calculated by using cyclic voltammetry. Boron-doped diamond networks with two different porosities of 16% (DN16) and 64% (DN64) were applied. Please note that the thickness of the boron-doped diamond networks is 3 μm, slightly lower than that of the undoped diamond networks shown above. The corresponding SEM images are shown in Figure S4 in Supporting Information. Figure 6a shows their cyclic voltammograms in 0.1 M H_2SO_4, along with that of the flat nanocrystalline diamond film. The currents at 0.15 V are 0.052, 8.33, and 25.5 μA for the flat diamond film, DN16, and DN64, respectively. It is known that the electrochemical background (or capacitive) current is proportional to the active surface area in contact with the electrolyte solution.[35] Assuming that the specific capacitance of diamond does not alter before and after wet-chemical etching, the effective surface area of DN16 and DN64 are ~160 and ~490 times higher than that of the flat nanocrystalline diamond film. It is noteworthy that the diamond networks measured here are half-closed. Even though the pores are relatively large in the present study (hundreds of nanometers, belonging to the macro-porous material) and the surface of the pores is hydrophilic after etching (due to oxidation), the pores might still be partially sealed by air, and the diffusion of the electrolyte into the pores will thus be difficult. In this context, its advantage in the surface area enhancement may not be fully reflected by the above measurement and needs further optimization in the future while handling the electrode.

DOI: 10.1021/am508851r
ACS Appl. Mater. Interfaces 2015, 7, 5384−5390

The calculated surface area enhancement of a porous material is dependent on its thickness. To compare the diamond networks with the porous diamond films reported in literatures, we normalized the enhancement of surface area with the thickness of the films. The results are summarized in Table 1. Our approach gives the highest normalized surface areas. Moreover, the double layer capacitance of DN64 was calculated as 13.7 F/g or 17.3 F/cm^3 at a scan rate of 100 mV/s (see Supporting Information for details), which is of the same order with that of carbon aerogel (77 F/cm^3)[36] and microporous carbon (80 F/cm^3).[37] After further optimization and proper decoration with other materials (i.e., MnO_2, NiO, and V_2O_5, etc.), diamond-network-based supercapacitors can even be constructed with a high power density and a long lifetime.

The electrochemical working potential (Figure S5, Supporting Information) of the diamond network remains similar to that of the flat nanocrystalline diamond film, implying the unchanged electrode activity of diamond network under water hydrolysis after etching. The electrochemical activity of diamond networks and the flat nanocrystalline diamond electrode was further examined by using the redox probe of $[Fe(CN)_6]^{3-/4-}$ in aqueous solution. The corresponding cyclic voltammograms (CV) of $[Fe(CN)_6]^{3-/4-}$ are shown in Figure 6b. Well-defined redox waves are seen on all electrodes. Nevertheless, the widest CV plots are observed on DN64 followed by DN16. This owes to their high capacitive currents, resulting from their large surface areas. ΔE (peak differences of anodic peak from cathodic one) and I_p^{ox}/I_p^{red} (the ratio of the anodic peak current, I_p^{ox}, to the cathodic peak current, I_p^{red}) are 90 mV and 1 for a flat diamond film, 116 mV and 1.1 for DN16, and 121 mV and 1.2 for DN64, respectively. Because $[Fe(CN)_6]^{3-/4-}$ redox reactions are surface-sensitive, the higher ΔE observed on the diamond networks is probably due to the oxidation of diamond surface during the etching process. The equal ratio of the peak currents implies that the oxidation and reduction of $[Fe(CN)_6]^{3-/4-}$ occur at a similar electron transfer rate on all considered films. The relationship between cathodic peak current of $[Fe(CN)_6]^{3-/4-}$ and square root of the scan rate is shown in Figure S6 (Supporting Information), which presents their proportionality on all electrodes. This relationship indicates that no undesired adsorption/reaction process occurred between the diamond networks and $[Fe(CN)_6]^{3-/4-}$. Its redox activity is thus controlled by the diffusion of the analyte. Moreover, the peak currents of $[Fe(CN)_6]^{3-/4-}$ on diamond networks are close to that on the flat diamond electrode. This similar behavior between diamond networks and the flat diamond results from the overlapping of diffusion layers on all pores (up to 1 μm). A similar phenomenon has also been observed in the case of diamond nanowire arrays.[35] All the above results suggest that the diamond networks maintain good electrochemical properties of bulk diamond. They are thus excellent and promising electrode materials with large surface area. Consequently, the diamond networks will be a potential platform for electrochemical applications. In the present study, even though the size of the diamond network is only 1 × 0.5 cm^2, it is possible to be scaled (i.e., up to 2 in., depending on the size of the wafer for depositing the composite films). Moreover, the present approach is a template-free approach. Compared to the other template-based methods, it reduces the complexities and the cost during fabrication, which is favorable for industrial application and beneficial for its further translation. Furthermore, by introducing a bias-assisted composite film deposition, the distribution of the β-SiC phase in the film can be further controlled to achieve a nanometer-scale distribution. In this case, diamond networks with nanometer-sized pores may even be possible and its application in lithium-free batteries or biofiltrations may be evoked. However, the long etching duration could be a drawback of the current approach, which requires further investigation to explore a more efficient etching process.

CONCLUSIONS

Diamond networks, the porous diamond with both vertically and horizontally interconnected pores, have been fabricated using a simple template-free approach. Experimentally, it was conducted by a selective removal of β-SiC phase from diamond/β-SiC composite films. The etching rate was determined to be ~50 nm/h. The porosity has been designed through varying the ratios of the β-SiC phase in the composite during preparation of composite films. The porosities were tunable in the range of 15−68%. Electrochemical analysis reveals that diamond networks maintain excellent electrochemical properties of diamond, regardless of their different porosities. For a 3 μm thick diamond network with a porosity of 64%, a surface area enhancement of ~490 fold has been achieved. These diamond networks are promising candidates for applications in the fields of water filtering, super capacitors, catalyst−supports, and so on. More details are required in the future regarding its local functionalization as well as its size/shape related properties.

ASSOCIATED CONTENT

Supporting Information

SEM and TEM images of the composite film before and after etching, composite films deposited with different TMS/CH_4 ratios, SEM images of boron doped composite film and diamond networks, electrochemical working potential of nanocrystalline diamond film and the diamond network, detailed calculation of the double layer capacitance of DN64 and peak currents vs square root of scan rate of different films. This material is available free of charge via the Internet at http://pubs.acs.org.

AUTHOR INFORMATION

Corresponding Author

*Tel.: +49 271 7402966. Fax: + 49 271 740 2442. E-mail: xin.jiang@uni-siegen.de.

Notes

The authors declare no competing financial interest.

ACKNOWLEDGMENTS

The authors thank Dr. Rainer Bornemann for his help for recording Raman spectra.

REFERENCES

(1) Li, Y.; Fu, Z.-Y.; Su, B.-L. Hierarchically Structured Porous Materials for Energy Conversion and Storage. *Adv. Funct. Mater.* **2012**, *22*, 4634−4667.

(2) Wang, D.-W.; Li, F.; Liu, M.; Lu, G. Q.; Cheng, H.-M. 3D Aperiodic Hierarchical Porous Graphitic Carbon Material for High-Rate Electrochemical Capacitive Energy Storage. *Angew. Chem., Int. Ed.* **2007**, *47*, 373−376.

(3) Lei, W. W.; Portehault, D.; Liu, D.; Qin, S.; Chen, Y. Porous Boron Nitride Nanosheets for Effective Water Cleaning. *Nat. Commun.* **2013**, *4*, 1777.

DOI: 10.1021/am508851r
ACS Appl. Mater. Interfaces 2015, 7, 5384−5390

(4) Valtchev, V.; Tosheva, L. Porous Nanosized Particles: Preparation, Properties, and Applications. *Chem. Rev.* **2013**, *113*, 6734−6760.
(5) Pera-Titus, M. Porous Inorganic Membranes for CO_2 Capture: Present and Prospects. *Chem. Rev.* **2014**, *114*, 1413−1492.
(6) Erri, P.; Nader, J.; Varma, A. Controlling Combustion Wave Propagation for Transition Metal/Alloy/Cermet Foam Synthesis. *Adv. Mater.* **2008**, *20*, 1243−1245.
(7) Zhang, Q.; Zhang, T.; Ge, J.; Yin, Y. Permeable Silica Shell through Surface-Protected Etching. *Nano Lett.* **2008**, *8*, 2867−2871.
(8) Wu, D.; Xu, F.; Sun, B.; Fu, R.; He, H.; Matyjaszewski, K. Design and Preparation of Porous Polymers. *Chem. Rev.* **2012**, *112*, 3959−4015.
(9) Lee, W.; Park, S. J. Porous Anodic Aluminum Oxide: Anodization and Templated Synthesis of Functional Nanostructures. *Chem. Rev.* **2014**, *114*, 7487−7556.
(10) Li, Y.; Yu, J. New Stories of Zeolite Structures: their Descriptions, Determinations, Predictions, and Evaluations. *Chem. Rev.* **2014**, *114*, 7268−7316.
(11) Nebel, C. E.; Ristein, W. *Thin Film Diamond: I*; Elsevier: Amsterdam, 2003.
(12) Nebel, C. E.; Ristein, W. *Thin Film Diamond: II*; Elsevier: Amsterdam, 2003.
(13) Mammana, V. P.; Mansano, R. D.; Verdonck, P.; Pavani Filho, A.; Salvadori, M. C. Diamond Membranes with Controlled Porosity. *Diamond Relat. Mater.* **1997**, *6*, 1824−1829.
(14) Mammana, V. P.; Silva, S.; Mansano, R. D.; Verdonck, P.; Filho, A. P.; Salvadori, M. C.; Brown, I. G. Porous Freestanding Diamond Membranes with Reduced Pore Diameter. *Thin Solid Films* **1999**, *353*, 239−243.
(15) Arora, S. K.; Chhoker, S.; Sharma, N. K.; Singh, V. N.; Vankar, V. D. Growth and Field Emission Characteristics of Diamond Films on Macroporous Silicon Substrate. *J. Appl. Phys.* **2008**, *104*, 103524.
(16) Braga, N. A.; Cairo, C. A. A.; Matsushima, J. T.; Baldan, M. R.; Ferreira, N. G. Diamond/Porous Titanium Three-Dimensional Hybrid Electrodes. *J. Solid State Electrochem.* **2010**, *14*, 313−321.
(17) Zanin, H.; May, P. W.; Fermin, D. J.; Plana, D.; Vieira, S. M. C.; Milne, W. I.; Corat, E. J. Porous Boron-Doped Diamond/Carbon Nanotube Electrodes. *ACS Appl. Mater. Interfaces* **2013**, *6*, 990−995.
(18) Ralchenko, V. G.; Sovyk, D. N.; Bolshakov, A. P.; Homich, A. A.; Vlasov, I. I.; Kurdyukov, D. A.; Golubev, V. G.; Zakhidov, A. A. Diamond Direct and Inverse Opal Matrices Produced by Chemical Vapor Deposition. *Phys. Solid State* **2011**, *53*, 1131−1134.
(19) Kurdyukov, D. A.; Feoktistov, N. A.; Nashchekin, A. V.; Zadiranov, Y. M.; Aleksenskii, A. E.; Vul, A. Y.; Golubev, V. G. Ordered Porous Diamond Films Fabricated by Colloidal Crystal Templating. *Nanotechnology* **2012**, *23*, 015601.
(20) Honda, K.; Rao, T. N.; Tryk, D. A.; Fujishima, A.; Watanabe, M.; Yasui, K.; Masuda, H. Electrochemical Characterization of the Nanoporous Honeycomb Diamond Electrode as an Electrical Double-Layer Capacitor. *J. Electrochem. Soc.* **2000**, *147*, 659−664.
(21) Sakaue, H.; Yoshimura, N.; Shingubara, S.; Takahagi, T. Low Dielectric Constant Porous Diamond Films Formed by Diamond Nanoparticles. *Appl. Phys. Lett.* **2003**, *83*, 2226−2228.
(22) Kriele, A.; Williams, O. A.; Wolfer, M.; Hees, J. J.; Smirnov, W.; Nebel, C. E. Formation of Nano-Pores in Nanocrystalline Diamond Films. *Chem. Phys. Lett.* **2011**, *507*, 253−259.
(23) Cambaz, G. Z.; Yushin, G. N.; Gogotsi, Y.; Lutsenko, V. G. Anisotropic Etching of SiC Whiskers. *Nano Lett.* **2005**, *6*, 548−551.
(24) Roper, C. S.; Howe, R. T.; Maboudian, R. Room-Temperature Wet Etching of Polycrystalline and Nanocrystalline Silicon Carbide Thin Films with HF and HNO_3. *J. Electrochem. Soc.* **2009**, *156*, D104−D107.
(25) Shi, Y. L.; Tan, M. H.; Jiang, X. Deposition of Diamond/β-SiC Gradient Composite Films by Microwave Plasma-assisted Chemical Vapor Deposition. *J. Mater. Res.* **2002**, *17*, 1241−1243.
(26) Zhuang, H.; Zhang, L.; Staedler, T.; Jiang, X. Highly Selective Diamond and β-SiC Crystal Formation at Increased Atomic Hydrogen Concentration: A Route for Synthesis of High-quality and Patterned Hybrid Diamond/β-SiC Composite Film. *Scr. Mater.* **2011**, *65*, 548−551.
(27) Jiang, X.; Klages, C. P. Synthesis of Diamond/β-SiC Composite Films by Microwave Plasma Assisted Chemical Vapor Deposition. *Appl. Phys. Lett.* **1992**, *61*, 1629−1631.
(28) Lee, J.; Kim, J.; Hyeon, T. Recent Progress in the Synthesis of Porous Carbon Materials. *Adv. Mater.* **2006**, *18*, 2073−2094.
(29) Prawer, S.; Nemanich, R. J. Raman Spectroscopy of Diamond and Doped Diamond. *Philos. Trans. R. Soc., A* **2004**, *362*, 2537−2565.
(30) Zhuang, H.; Song, B.; Srikanth, V. V. S. S.; Jiang, X.; Schönherr, H. Controlled Wettability of Diamond/β-SiC Composite Thin Films for Biosensoric Applications. *J. Phys. Chem. C* **2010**, *114*, 20207−20212.
(31) Zhuang, H.; Jiang, X. Growth Controlling of Diamond and β-SiC Microcrystals in the Diamond/β-SiC Composite Films. *Surf. Coat. Technol.* **2014**, *249*, 84−89.
(32) Srikanth, V.; Tan, M. H.; Jiang, X. Initial Growth of Nanocrystalline Diamond/β-SiC Composite Films: A Competitive Deposition Process. *Appl. Phys. Lett.* **2006**, *88*, 073109.
(33) Gao, F.; Wolfer, M. T.; Nebel, C. E. Highly Porous Diamond Foam as a Thin-Film Micro-Supercapacitor Material. *Carbon* **2014**, *80*, 833−840.
(34) Zhuang, H.; Fu, H.; Jiang, X. Selective Secondary Nucleation Controlled (001)-Texture in Boron Doped Diamond Films by Increasing the Concentrations of Tetramethylsilane and Trimethylborane. *Surf. Coat. Technol.* **2014**, *259*, 526−531.
(35) Brillas, E.; Martinez-Huitle, C. A. *Synthetic Diamond Films: Preparation, Electrochemistry, Characterization And Applications*; John Wiley & Sons, Inc.: Hoboken, NJ, 2011.
(36) Li, W.; Pröbstle, H.; Fricke, J. Electrochemical Behavior of Mixed C_mRF Based Carbon Aerogels as Electrode Materials for Supercapacitors. *J. Non-Cryst. Solids* **2003**, *325*, 1−5.
(37) Simon, P.; Gogotsi, Y. Materials for Electrochemical Capacitors. *Nat. Mater.* **2008**, *7*, 845−854.

DOI: 10.1021/am508851r
ACS Appl. Mater. Interfaces 2015, 7, 5384−5390